Int. J. Environ. Sci. Technol. (2016) 13:1393–1404
DOI 10.1007/s13762-016-0960-0

ORIGINAL PAPER

# Adsorption kinetics and thermodynamics of organophosphorus profenofos pesticide onto Fe/Ni bimetallic nanoparticles

**N. Mansouriieh[1] · M. R. Sohrabi[1] · M. Khosravi[1]**

Received: 1 October 2015 / Revised: 30 January 2016 / Accepted: 10 February 2016 / Published online: 1 March 2016


**Abstract** Bimetallic Fe/Ni nanoparticles were synthesized and used for the removal of profenofos organophosphorus pesticide from aqueous solution. These novel bimetallic nanoparticles (Fe/Ni) were characterized by scanning electron microscopy, energy-dispersive X-ray analysis spectroscopy, X-ray diffraction, and Fourier transform infrared spectroscopy. The effect of the parameters of initial pesticide concentration, pH of the solution, adsorbent dosage, temperature, and contact time on adsorption was investigated. The adsorbent exhibited high efficiency for profenofos adsorption, and equilibrium was achieved in 8 min. The Langmuir, Freundlich, and Temkin isotherm models were used to determine equilibrium. The Langmuir model showed the best fit with the experimental data ($R^2 = 0.9988$). Pseudo-first-order, pseudo-second-order, and intra-particle diffusion models were tested to determine absorption kinetics. The pseudo-second-order model provided the best correlation with the results ($R^2 = 0.99936$). The changes in the thermodynamic parameters of Gibb's free energy, enthalpy, and entropy of the adsorption process were also evaluated. Thermodynamic parameters indicate that profenofos adsorption using Fe/Ni nanoparticles is a spontaneous and endothermic process. The value of the activation energy ($E_a = 109.57$ kJ/mol) confirms the nature of the chemisorption of profenofos onto Fe/Ni adsorbent.

**Keywords** Chemisorption · Environmental remediation · Isotherm model · Thermodynamic parameters

✉ N. Mansouriieh
nafismansouriieh@gmail.com

[1] Department of Chemistry, Islamic Azad University, North Tehran Branch, P.O. Box 1913674711, Tehran, Islamic Republic of Iran

## Introduction

Pesticides are chemical and biological substances used to control weeds, insects, and other pests and minimize loss for agricultural products. Despite their important role in agriculture, unsystematic utilization of chemical pesticides causes significant environmental problems (Meyer 2005). Organophosphates are widely used as insecticides and acaricides (Edwards 1973). Research has determined that the agricultural runoff is the main source of pesticide, and under suitable environmental conditions, they can persist long term in environmental compartments (Ali and Jain 2001; Ragnarsdottir 2000). These compounds are hazardous to the environment (Gallo and Lawryk 1988).

Profenofos (PFF) is a highly active organophosphorous pesticide (OPP). Long-term exposure to water polluted with PFF is harmful to human health. OPPs significantly inhibit acetylcholinesterase activity and promote instability of the erythrocyte membrane (Shi et al. 2012). Acetylcholinesterase inhibition in the nervous system inhibits respiratory, myocardial, and neuromuscular transmission, which are acute toxicologic effects of OPPs (Perera et al. 2003). Recently, environmental concerns associated with the aggregation of OPPs in food products and water supplies have focused efforts on expanding safe, accessible, and economically feasible methods for detoxification (Mahboob et al 2013; Sunitha et al 2007). PFF residue in drinking groundwater resources of rural areas in the northwest of Iran, water and sediments of River Ravi in Pakistan is reported (Shakerkhatibi et al 2014; Mahboob et al 2013). Wastewater containing OPPs cannot be treated efficiently by biological techniques. The toxicity of PFF for microorganisms makes its biodegradation impossible (Hincapie et al 2005). Figure 1 shows the chemical structure of PFF.

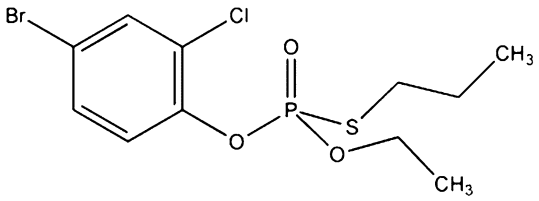


**Fig. 1** Chemical structure of PFF

The adsorption technique is one of the most efficient and promising methods for the removal of pollutants from wastewater due to its inexpensiveness, and ease of operation the adsorbents (Ali 2010, 2012; Ali and Gupta 2006; Ali et al 2012; Ali 2014). Currently, several adsorption approaches are being used to remove organic and inorganic pollutants from aqueous effluents, including phenol removal and recovery (Gupta et al 1998), dye removal using carbon nanotubes (Gupta et al 2013), heavy metals remediation (Gupta et al 2015), pesticides removal from wastewater by activated carbon prepared from waste rubber tire and bagasse fly ash (Gupta et al 2011; Gupta and Ali 2001).

Nanoscale zero-valent iron (nZVI) is a powerful alternative reducing agent that is easily accessible, effectively degrades pollutants, and generates very little waste and secondary pollutants (Gillham and O'Hannesin 1994). Furthermore, application of nZVI for environmental remediation has increased because of its smaller particle size, large specific surface area, higher density of reactive surface sites, and greater intrinsic reactivity of surface sites (Theron et al 2008).

These nanoparticles have been used for remediation of organic contaminants such as halogenated organics (Xu et al 2014) and dyes (Sohrabi et al. 2015; Zhang et al. 2011). The nZVI particles tend to react with surrounding media or agglomerate into larger particles in response to its high surface energy and intrinsic magnetic interaction, which results in significant loss of reactivity (Phenrat et al. 2007). The nZVI particles easily oxidize or ignite spontaneously when exposed to air (Ponder et al. 2000), which lowers its chemical reactivity to iron oxide formation. Attempts have been made to increase the efficiency of the redox reaction by decreasing the inactivation effects of the passivation layer (Huguet and Marshall 2009). Coating nZVI with a metal such as Ag, Pd, Pt, and Ni produces bimetallic nanoparticles. These are an efficient approach which serves as a protective agent against corrosion of the iron surface (Huguet and Marshall 2009). The prevention or reduction in the formation and accumulation of toxic by-products is the additional advantage of bimetallic nanoparticles (Hosseini et al. 2011). Despite the fact that Ni having a weaker catalytic effect compared to Pd and others, its good stability and lower cost make it more suitable for wastewater treatment (Xu et al. 2005).

Several authors have studied different properties of PFF pesticide such as their degradation and aggregation in wastewater. Cordeiro studied the PFF degradation in an electrochemical flow reactor using boron-doped diamond anodes (2013). Furthermore, Jabeen studied the PFF degradation by a bacterial consortium (2015).

The present study evaluated the efficiency of bimetallic Fe/Ni nanoparticles for the removal of PFF pesticide from aqueous solution. Knowledge about the kinetic and mass transfer processes of the adsorption treatment system is essential to its design. The present study reports on the applicability of thermodynamics for the adsorption of profenofos pesticide.

## Materials and methods

### Materials

The following materials employed in this study were purchased from Merck (Germany): sodium borohydride ($NaBH_4$), ferric chloride hexahydrate ($FeCl_36H_2O$), and nickel (II) nitrate hexahydrate ($Ni(NO_3)_2.6H_2O$). Sodium hydroxide (NaOH) and hydrochloric acid (HCl) were used for pH adjustment and were purchased from Merck (Germany). All other chemicals were of analytical grade. Profenofos (molecular formula: $C_{11}H_{15}BrClO_3PS$) with a molar mass of 373.63 and 400 (g/l) was purchased from National Farmer Chemicals (Iran).

### Preparation of Fe/Ni bimetallic nanoparticles

The nZVI particles used in this study were chemically synthesized using liquid-phase reduction (Frost et al. 2010). The experiments were carried out applying $N_2$ atmosphere, and all the aqueous solutions were prepared with the distilled, deionized water (DDW). Sodium borohydride solution (100 ml, 0.3 M) was added at the speed of 1–2 drops per second drop wise into ferric chloride solution (250 ml, 0.1 M), and the product was mixed vigorously using a mechanical stirrer. The resulting reaction is (Sun et al. 2007):

$$4Fe^{3+}_{(aq)} + 3BH^{-}_{4(aq)} + 9H_2O \rightarrow 4Fe^{0}_{(s)} + 3H_2BO^{-}_{3(aq)} + 12H^{+}_{(aq)} + 6H_{2(g)} \quad (1)$$

Black particles of nZVI appeared immediately after introducing the first drop of $NaBH_4$ solution. The generated iron particles were separated and washed with DDW. To prepare the bimetallic Fe/Ni nanoparticles, specific amounts of freshly prepared nZVI and Ni $(NO_3)_2{\cdot}6H_2O$

**Table 1** Isotherm constants for the adsorption of PFF onto Fe/Ni bimetallic nanoparticles ([PFF] = 0.6 mg/l; Fe/Ni dosage 1 g/l; pH = 5.73; room temperature) (±95 % confidence level)

| Model | $R^2$ | $R^2_{adj}$ | $S^2$ | *RMSD* | Parameters | Parameter values |
|---|---|---|---|---|---|---|
| 2-p Langmuir | 0.9988459 | 0.9984613 | 0.0029568 | 0.0188366 | $q_m$ (mg/g) | 0.202045 |
| | | | | | $K_L$ (L/mg) | 11.90616 |
| 2-p Freundlich | 0.897612 | 0.8634826 | 0.0008412 | 0.0100472 | $K_F$ (mg/g) | 0.187702 |
| | | | | | $n$ | 6.85401 |
| 2-p Temkin | 0.9092115 | 0.8789487 | 2.131E−05 | 0.001599 | $RT/\Delta Q$ | 0.0248 |
| | | | | | $K_T$ (L/mg) | 1913.046 |

(5 wt%) were stirred in 250 ml DDW for 20 min at room temperature. The process is represented by the following equation:

$$Fe_{(s)} + Ni^{2+} \rightarrow Fe^{2+} + Ni(s) \quad (2)$$

Separation and washing were similar to the process for nZVI. Fe/Ni bimetallic nanoparticles were dried under N2 atmosphere.

## Characterizations and methods

Scanning electron microscopy (SEM) and energy-dispersive X-ray analysis (EDAX) (Philips, ESEM, XL 30) were used to characterize the Fe/Ni bimetallic nanoparticles, the morphology, size and surface chemical composition, respectively.

X-ray powder diffraction (XRD) was performed using a Cu Kα radiation to determine the composition of the newly synthesized Fe/Ni bimetallic nanoparticles. The accelerating voltage was 40 kV and applied current was 30 mA.

FTIR spectra of Fe/Ni nanoparticles before and after reacting with PFF were obtained using Fourier transform infrared spectroscope (FTIR Nicolet 8700, Thermo Scientific). Samples for FTIR measurement were prepared by mixing 1 % (W/W) specimen with 100 mg of KBr powder and pressed into a sheer slice. A spectral resolution of 2 $cm^{-1}$ and average of 32 scans were used for each measurement. The reaction was followed by double-beam UV–Vis spectrometry using a 1-cm quartz cell (Cary 100; Varian) at $\lambda = 263$ nm.

PFF residue analysis was accomplished using mass spectrometry (MS/MS-Agilent G6410) equipped with triple quadrupole mass spectrometer in positive ESI mode.

## PFF adsorption studies using Fe/Ni bimetallic nanoparticles

Adsorption of PFF by Fe/Ni bimetallic nanoparticles was carried out using the batch method, and the influence of contact time (2–20 min), adsorbent dosage (7–17 g/l), pH (2–8.36), initial pesticide concentration (0.6, 1, 1.2, and 1.4 mg/l), and temperature (298, 308, and 318 K) was studied. The adsorption measurements were taken by mixing various amounts of Fe/Ni bimetallic nanoparticles in glass Erlenmeyer flasks containing 100 ml of pesticide solution of known concentration. The pH of the solution was adjusted to the desired value by adding a small amount of HCl (0.1 M) or NaOH (0.1 M). At the end of determined time interval, samples were collected and the supernatant solution was separated from the Fe/Ni nanoparticles by centrifugation at 3000 rpm for 15 min. The adsorption capacity of PFF on the adsorbent was calculated as (Mourabet et al. 2014):

$$q_t = \frac{(C_0 - C_t)V}{W} \quad (3)$$

where $C_0$ is the initial PFF concentration in solution (mg/l), $C_t$ is the PFF concentration at $t$ min (mg/l), $V$ is the volume of pesticide (l), and $W$ is the weight of adsorbent (g).

The isotherm parameters were evaluated using Polymath 6.0 software and are shown in Table 1. The correlation coefficient ($R^2$) and adjusted correlation coefficient ($R^2_{adj}$) were used to determine whether a model correctly represents the data. The correlation coefficient approached one and was also close to ($R^2_{adj}$); thus, it was concluded that the regression model was correct. Variance ($S^2$) and root mean square error (RMSD) were used to compare the isotherm models for adsorption of PFF using Fe/Ni bimetallic nanoparticles. A model with less variance and RMSD more accurately portrays the data. The average observations of ($\bar{y}$), $R^2$, $R^2_{adj}$ values, RMSD, and $S^2$ were calculated using Eqs. (4–8), respectively:

$$\bar{y} = \frac{1}{n}\left(\sum_{i=1}^{n} y_{i_{obs}}\right) \quad (4)$$

$$R^2 = 1 - \frac{\sum_{i=1}^{n}(y_{i_{obs}} - y_{i_{calc}})^2}{\sum_{i=1}^{n}(y_{i_{obs}} - \bar{y})^2} \quad (5)$$

$$R^2_{adj} = 1 - \frac{(1 - R^2)(n-1)}{n-p} \quad (6)$$

$$RMSD = \frac{1}{n}\left(\sum_{i=1}^{n}(y_{i_{obs}} - y_{i_{calc}})^2\right)^{1/2} \quad (7)$$

$$S^2 = \frac{\sum_{i=1}^{n}(y_i - y)^2}{n-1} \quad (8)$$

where $n$ is the number of observations, $p$ is the independent variable, $y_i$ is a specific observation, *obs* denotes observed data, and calc denotes calculated data.

$R^2$, $R^2_{adj}$, $S^2$, and RMSD for each model were calculated at the 95 % confidence interval for PFF adsorption onto Fe/Ni bimetallic nanoparticles; the results are shown in Table 1.

## Experiment of nickel ion leaching

Ten 100-ml flasks were used in this experiment. In every flask, 0.5 g of Fe/Ni bimetallic nanoparticles (5 wt%) and 100 ml of PFF solution were added. The experiment conditions were as follows: temperature, 26 ± 2 °C; initial pH, 5.7; initial PFF concentration, 1 mg/l; Fe/Ni dosage, 1 g/l; speed of stirring, 200 rpm. Every 3 min, one flask was taken out and the solution was filtered by 0.45-μm filtration membrane. 1 ml of hydrochloric acid (1 mol/l) was added into the filtered solution. Then, the Ni content in the solution was analyzed by flame atomic absorption (PerkinElmer 2380).

## Results and discussion

### Characterization

Figure 2a shows the morphology and size of the nanoscaled bimetallic particles. The SEM image indicates that the Fe/Ni nanoparticles are approximately spherical and form chains resulting from the magnetic interaction between nanoparticles. The results show that the Fe/Ni particles are 20–60 nm in diameter, and the diameter of the particles is <60 nm. Figure 2b shows the results of EDAX analysis and indicates that Fe, Ni, and O are present on the nanoparticle surface. Figure 2c shows the XRD pattern of the Fe/Ni synthesized nanoparticles. An apparent peak at $2\theta = 44.9°$ indicates the presence of nZVI in the samples; however, the peak at 40.9° corresponds to iron and nickel due to face-centered cubic crystal structures, suggesting the possibility of Fe/Ni alloy formation (Brijesh et al. 2011). Also, the peak at $2\theta = 44.8°$ corresponds to Fe/Ni nanoparticles. Furthermore, iron oxide layers such as γ-$Fe_2O_3$ ($2\theta = 35.68°$) and $Fe_3O_4$ ($2\theta = 35.45°$) were formed on Fe/Ni nanoparticles (Wang and Zhu 2007; Weng et al. 2013). This can be explained by the corrosion of Fe as a reductant to form oxide of Fe (II) and Fe (III), and PFF adsorbed on iron oxides (Gupta and Nayak 2012). The average crystallite size evaluated from Schere equation confirmed SEM results. The FTIR spectra in the wave numbers ranging from 400 to 4000 $cm^{-1}$ regarding Fe/Ni nanoparticles, before and after reacting to PFF, are presented in Fig. 3a, b, respectively. As shown in the Fig. 3a, b, there are wide and large absorption bands around the 3400 $cm^{-1}$, which are mainly caused by the adsorbed water on the surface and stretching vibration of O–H in the $H_2O$ (Saleh and Gupta 2012a, b; Saleh and Gupta 2011). The absorption peaks at the bands around 668, 469, 708, and 795 $cm^{-1}$ corresponding to Fe–O stretches of $Fe_2O_3$ and $Fe_3O_4$ were observed in Fig. 3a, b which was consistent with the results obtained from XRD (Liu et al. 2013). As shown in Fig. 3b. the weak bands at 2962 $cm^{-1}$, characteristic of stretching of aliphatic C–H (Taha et al. 2014). The appeared peaks around 1471 and ~1300 were due to the various vibrations of $–CH_2$ and $–CH_3$ groups. The intense band at 1021 $cm^{-1}$ is due to stretching of P–$OCH_3$ group (Singhal et al. 2012), and P=O stretching frequency was appeared around 1229 (Upadhay et al. 2013). Results obtained from the FTIR spectra indicate the PFF adsorption using Fe/Ni bimetallic nanoparticles.

### Effect of contact time

The influence of contact time on the adsorption capacity of Fe/Ni bimetallic nanoparticles is depicted in Fig. 4a. Figure 4a shows that the adsorption of PFF increased as the time increased and attained saturation at about 8 min. Saturation of the absorption sites onto the absorbent during this time did not change PFF removal efficiency. The removal of adsorbate was rapid, but it gradually decreased over time until it reached equilibrium. An initial concentration of pesticide of 1 mg/l (Mane et al. 2007) was used to investigate the kinetics of adsorption. PFF degradation by bacterial consortium was reported less than 90 % in 5 days (Jabeen et al. 2015). However, Fe/Ni bimetallic nanoparticles show a good ability to remove PFF from aqueous solution, approximately 96 % removal after 16-min contact time.

### Effect of initial concentration

The effect of the initial concentration of PFF was varied from 0.6 to 1.4 mg/l at room temperature for all runs; the Fe/Ni nanoparticle content was fixed at 10 g/l. The PFF uptake mechanism is dependent on the initial concentration of PFF. Figure 4b shows that the adsorption of PFF increased as the initial concentration increased at lower concentrations of PFF. This was probably the result of a higher mass transfer driving force from the increase in the number of molecules competing for the available binding sites on the adsorbent as the initial concentration of PFF increases (Fan et al. 2011). This trend reversed at higher concentrations in the experimental range. This can be attributed to the decrease in the adsorption caused by the increase in PFF concentration after saturation of the binding sites.

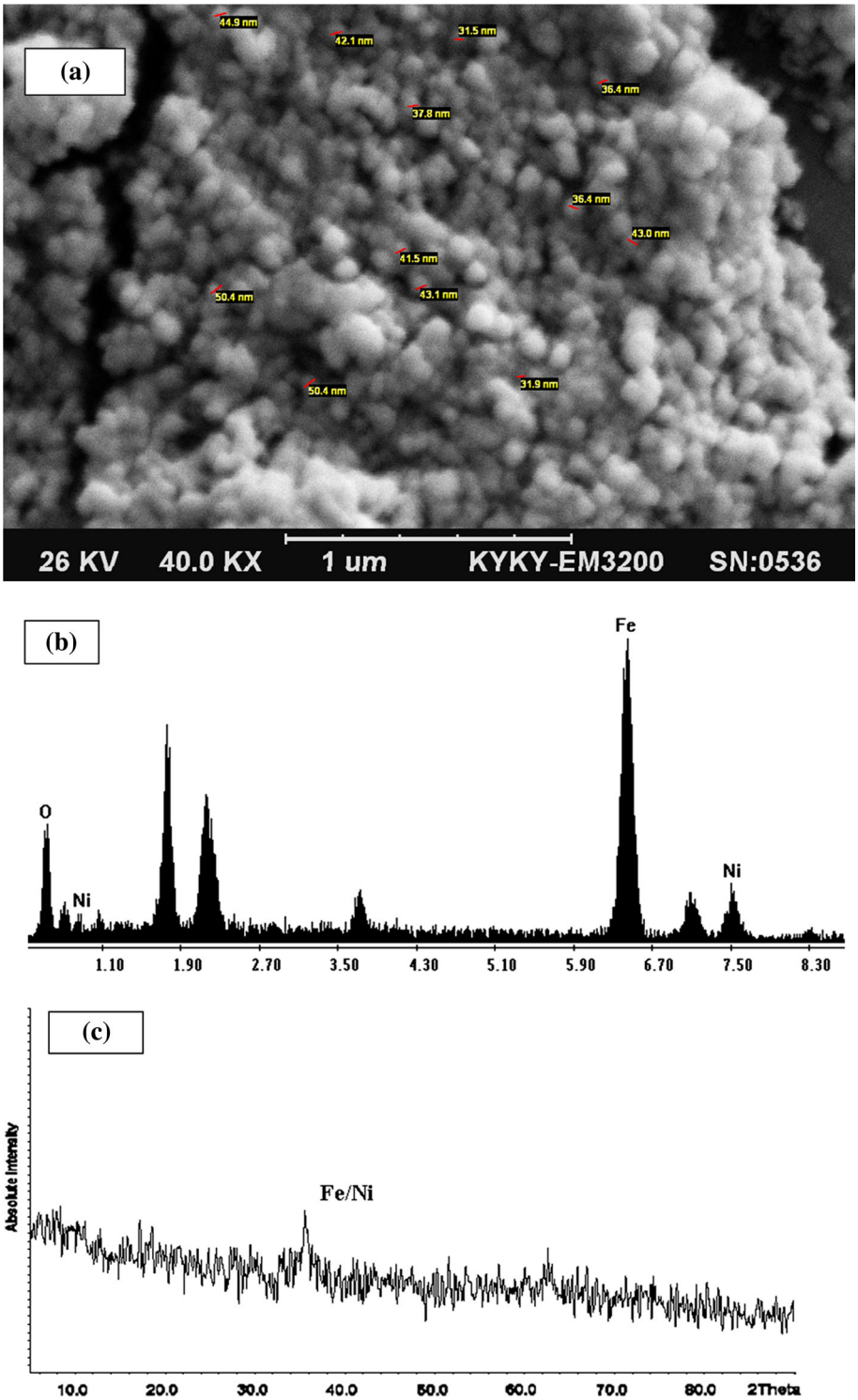


**Fig. 2** **a** SEM image, **b** EDAX spectra, **c** XRD pattern of Fe/Ni bimetallic nanoparticles

## Effect of initial pH

The effect of pH was investigated for an initial concentration of PFF at 1 mg/l and Fe/Ni nanoparticles concentration of 10 g/l. The initial pH values were adjusted using 0.1 M HCl and 0.1 M NaOH to form a series of pH values ranging from 2 to 8.36 (Fig. 4c). The adsorption capacity of the PFF increased as the pH of the solution increased from (2–7) and a maximum efficiency was observed at pH 7. However, adsorption capacity decreased by increasing

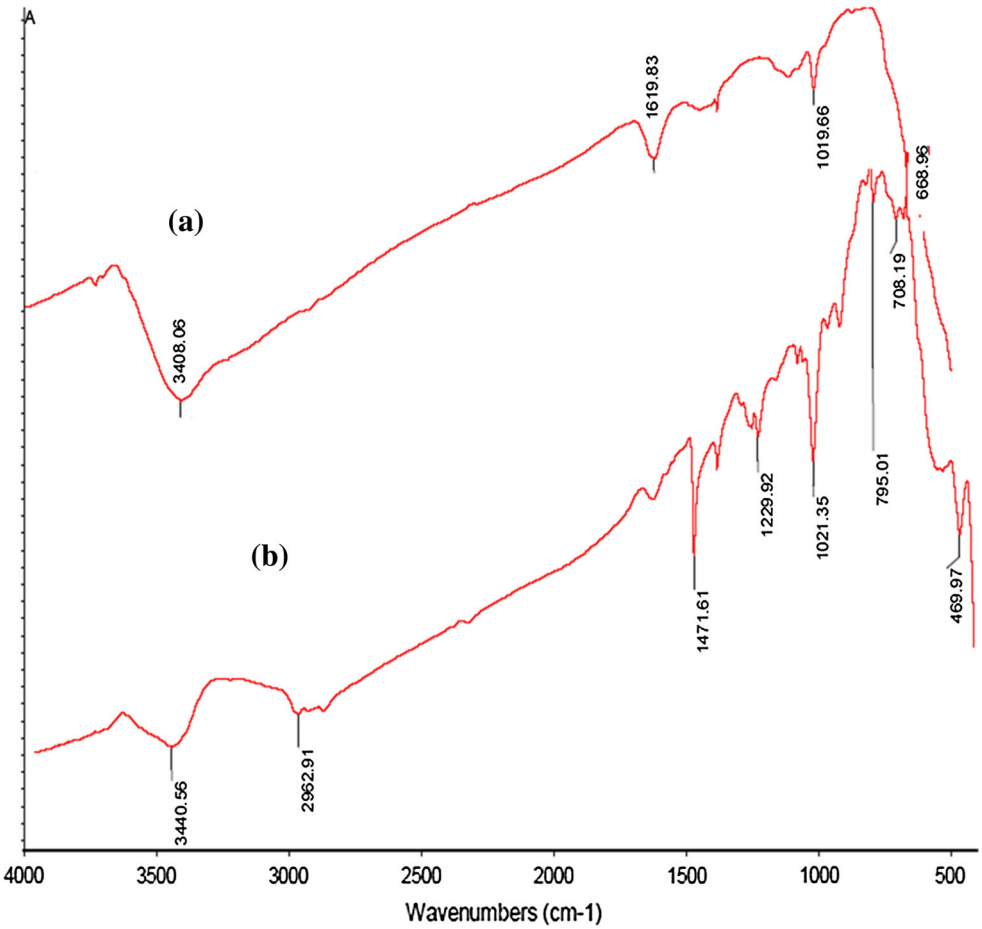


**Fig. 3** FTIR spectrum, **a** Fe/Ni bimetallic nanoparticles before reaction; **b** Fe/Ni nanoparticles after reaction

the pH to 8.36. This result could be attributed to the $pH_{zpc}$ (zero-point charge) of the Fe/Ni nanoparticles. The zero-point charge for Fe/Ni bimetallic nanoparticles was about 7.3. Thus, at pH < 7.3, the surface of Fe/bimetallic nanoparticles is relatively positive due to protonation (Saleh 2015a, b). The decrease in PFF removal with a decrease in pH from 5 to 2 can be attributed to protonation of the PFF molecules, repulsion forces from like charges (positive) on the catalyst surface, and PFF molecules with lower pH. Therefore, columbic or electrostatic interactions do not favor the sorption of PFF (Saleh et al. 2011). However, hydroxide precipitation formed gradually when the solution pH was high; this blanketed the Fe/Ni shell and decreased PFF adsorption (Sohrabi et al. 2015). Thus, the change in pH can influence the adsorption of PFF molecules on to the Fe/Ni nanocomposite surface. The adsorption is considered to be the important step for PFF removal (Saleh and Gupta 2012a, b).

## Effect of adsorbent dosage

The Fe/Ni nanoparticle concentration was varied from 0.7 to 1.7 g to study the effect of the adsorbent dose at room temperature. For all runs, the initial concentration of PFF was fixed at 1 mg/l. Fig. 4d shows the effect of Fe/Ni dosage on PFF adsorption. The adsorption efficiency increased as the adsorbent dosage increased. This was likely the result of the increased surface area and adsorption sites for the constant number of PFF molecules (Ozacar and Sengil 2005; Rasoulifard et al. 2010). Figure 4d indicates that the adsorption capacity of Fe/Ni nanoparticles decreased as the adsorbent dosage increased to above 8 g/l Fe/Ni. This decrease could be the result of aggregation at the adsorbent surface and an increase in diffusion path length (Gonen and Serin 2012; Ozacar and Sengil 2005).

## Effect of temperature

Temperature was varied from 298 to 318 K to study the effect of temperature on PFF adsorption (Fig. 4e). The adsorption capacity of PFF onto Fe/Ni nanoparticles increased slightly as temperature increased, indicating that the process is endothermic. This can be explained by the increased adsorptive interaction between the active sites on the adsorbent and the adsorbate ions (Dogan and Alkan 2003).

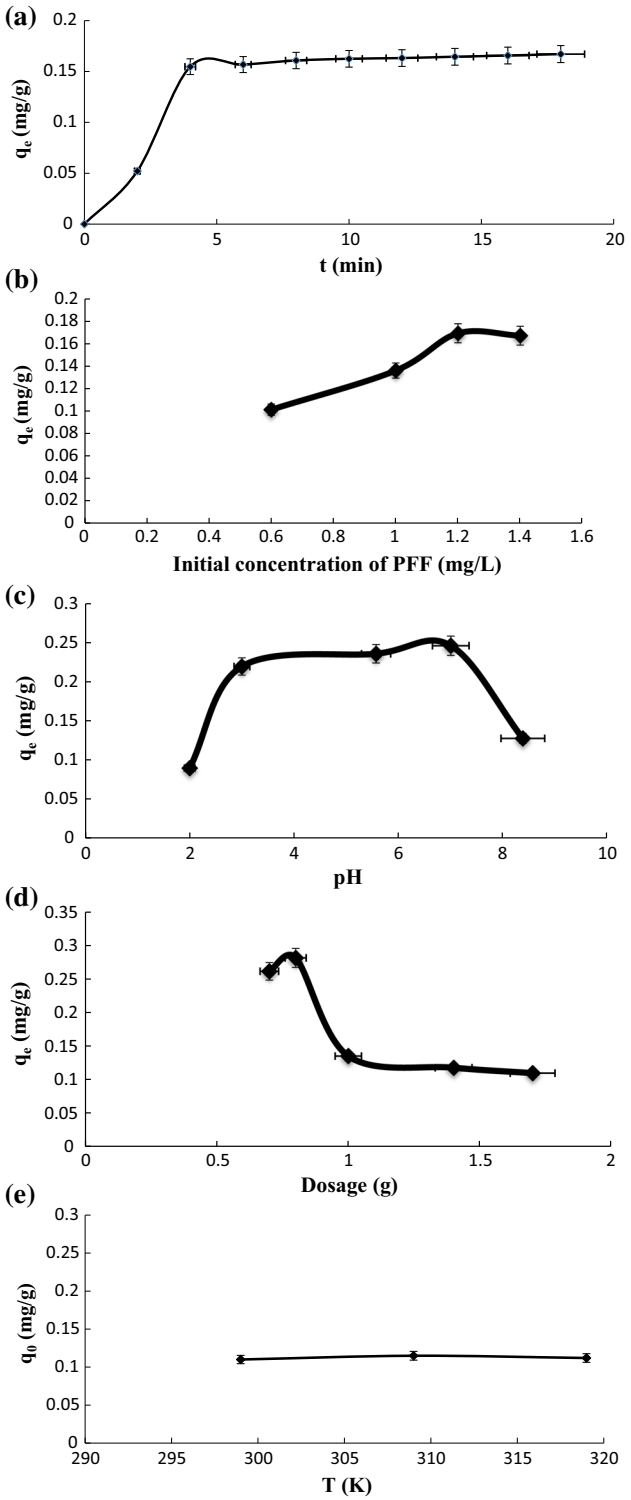


**Fig. 4** Condition affecting the adsorption of profenofos: **a** effect of contact time, **b** effect of PFF initial concentration, **c** effect of pH, **d** effect of dosage, and **e** effect of temperature

## Adsorption isotherms

The equilibrium adsorption isotherm is essential to understanding the mechanism of the adsorption systems. The Langmuir, Freundlich, and Temkin isotherm equations were used to interpret the experimental data.

### *Langmuir isotherm*

The Langmuir isotherm (Hameed 2009) theory is based on the assumption that adsorption on the homogeneous surface, i.e., the surface, consists of the identical sites equally available for adsorption and with equal energies of adsorption. The adsorbent becomes saturated after one layer of adsorbate molecules forms on the surface (Walker and Weatherley 2001). The linearized form of the Langmuir adsorption isotherm equation is:

$$\frac{C_e}{q_e} = \frac{1}{K_L q_m} + \frac{C_e}{q_m} \tag{9}$$

where $C_e$ is the equilibrium concentration of the solute (mg/l); $q_e$ is the equilibrium adsorption capacity (mg/g); $q_m$ is the maximum adsorption capacity (mg/g); and $K_L$ is the Langmuir adsorption model constant (L/mg).

Figure 4a shows the Langmuir adsorption isotherm for PFF onto Fe/Ni nanoparticles. As shown in Fig. 5a and Table 1, the Langmuir isotherm fits quite well with the experimental data ($R^2 = 0.9988459$). The maximum adsorption capacity ($q_m$) for this model was 0.2020 mg/g at 298 K. The Langmuir isotherm may fit the experimental data well because of the homogeneous distribution of active sites on the surface of the Fe/Ni, since the Langmuir equation assumes that the surface is homogenous.

The essential characteristics of the Langmuir isotherm can be expressed in terms of a dimensionless constant separation factor, or equilibrium parameter $R_L$, which is defined as (Hall et al. 1966):

$$R_L = \frac{1}{1 + KC_0} \tag{10}$$

The value of $R_L$ indicates that the isotherm is either irreversible ($R_L = 0$), favorable ($0 < R_L < 1$), linear ($R_L = 1$), or unfavorable ($R_L > 1$), where $C_0$ and $K$ are initial concentrations of PFF and Langmuir adsorption model constant, respectively. Figure 5b plots the separation factor at different concentrations and indicates that the adsorption of PFF using Fe/Ni nanoparticles is favorable at all equilibrium concentrations.

### *Freundlich isotherm*

Freundlich isotherm is an empirical equation that represents adsorption on heterogeneous surfaces. It assumes that increases in adsorbate concentration increase the concentration of the adsorbate onto the adsorbent surface. This isotherm model is applicable for both multilayer (physisorption) adsorption and monolayer (chemisorption)

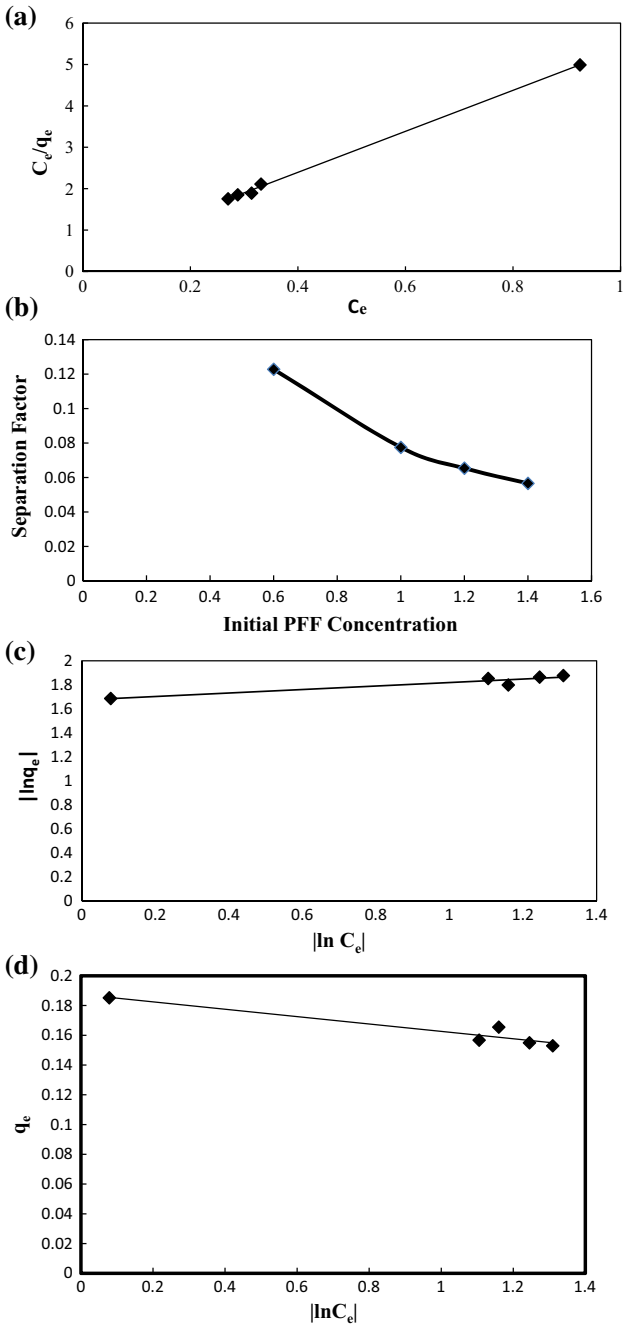


**Fig. 5** Plots of **a** Langmuir isotherm. **b** Separation factor for different initial PFF concentrations. **c** Freundlich isotherm. and **d** Temkin isotherm for PFF adsorption onto Fe/Ni bimetallic nanoparticles

adsorption (Boparai et al. 2011). The linearized Freundlich isotherm is given as:

$$\ln q_e = \ln K_f + \frac{1}{n} \ln C_e \tag{11}$$

where $C_e$ is the equilibrium concentration of the solute (mg/l), and $q_e$ is the equilibrium adsorption capacity (mg/g). Freundlich isotherm constant $K_f$ denotes the quantity of adsorbate adsorbed onto the adsorbent for a unit equilibrium concentration, and the value $(\frac{1}{n})$ indicates the heterogeneity of the system. In general, values for $n$ in the range of 1–10 indicate that the adsorbate was favorably adsorbed onto the adsorbent; $n < 1$ indicates that the adsorbate was inadequately adsorbed onto the adsorbent (Gupta et al. 2007).

The results from Freundlich analysis are shown in Table 1 and indicate that PFF was favorably adsorbed onto the Fe/Ni nanoparticles. Figure 5c shows the Freundlich isotherm of PFF onto the Fe/Ni nanoparticles. $R^2$ for this isotherm (0.897612) was not close enough to 1 and indicates that the Freundlich isotherm could not predict the experimental data.

*Temkin isotherm*

The Temkin isotherm assumes that the heat of adsorption of all molecules in the layer decreases linearly with coverage in response to adsorbent–adsorbate interaction and that adsorption is characterized by the uniform distribution of the binding energies up to a maximum binding energy. The linearized equation is (Temkin and Pyzhev 1940):

$$q_e = B \ln K_T + B \ln C_e \tag{12}$$

where $C_e$ is the equilibrium concentration of solute (mg/l), $q_e$ is the equilibrium adsorption capacity (mg/g), $B = \frac{RT}{\Delta Q}$ denotes the heat of adsorption, $T$ is the absolute temperature (K), $R$ is the universal gas constant (g/g mol K), $\Delta Q$ is the heat of adsorption (J), and $K_T$ is the equilibrium binding constant (l/mg). Figure 5d shows the Temkin isotherm of the PFF adsorption onto Fe/Ni nanoparticles. The value of $R^2 = 0.9092$ in Table 1 indicates that the Temkin model did not fit well the experimental data for adsorption of PFF.

## Adsorption kinetics

The pseudo-first-order, pseudo-second-order, and intra-particle diffusion models were applied to the data to analyze the adsorption kinetics of PFF. All the parameters of the pseudo-first-order and pseudo-second-order adsorption kinetic models and the intra-particle diffusion model were determined using Polymath 6.0 and are listed in Table 2. For the isotherm studies, to determine the goodness of fit, $R^2$, $R^2_{adj}$, $S^2$, and RMSD were calculated and are shown in Table 2. All parameters were calculated at the 95 % confidence interval. The plots of the experimental data and results obtained from two kinetic models and intra-particle diffusion are shown in Fig. 6a–c.

**Table 2** Kinetic parameters for the adsorption of PFF onto Fe/Ni bimetallic nanoparticles (Fe/Ni dosage 1 g/l; pH = 5.73; room temperature)

| | Initial concentration (mg/L) | | | |
|---|---|---|---|---|
| | 0.6 | 1 | 1.2 | 1.4 |
| *Pseudo-first-order kinetic model* | | | | |
| $k_1$ (1/min) | 0.734 | 0.6991607 | 0.665609 | 0.6068426 |
| $q_{e,cal}$ (mg/g) | 0.08192 | 0.2798 | 0.149733 | 0.102863 |
| $R^2$ | 0.9690866 | 0.8897005 | 0.9977681 | 0.9098745 |
| $R^2_{adj}$ | 0.9536299 | 0.8345507 | 0.9966522 | 0.8648118 |
| $S^2$ | 0.1718912 | 0.6060154 | 0.0099101 | 0.3647692 |
| *RMSD* | 0.1465824 | 0.2752307 | 0.035196 | 0.2135325 |
| *Pseudo-second-order kinetic model* | | | | |
| $k_2$ (g/mg min) | 22.834 | 15.03445 | 5.691604 | 12.18125 |
| $q_{e,cal}$ (mg/g) | 0.1125 | 0.168581 | 0.1787 | 0.169334 |
| $R^2$ | 0.9999515 | 0.9998839 | 0.9993638 | 0.9995028 |
| $R^2_{adj}$ | 0.999394 | 0.9998452 | 0.9992047 | 0.9993785 |
| $S^2$ | 0.0669652 | 0.0544826 | 0.3488673 | 0.3035755 |
| *RMSD* | 0.0862588 | 0.0808574 | 0.1968833 | 0.183659 |
| *Intra-particle diffusion model* | | | | |
| $K_i$ | 0.006560 | 0.0062753 | 0.021394 | 0.0102832 |
| $C$ (mg/g) | 0.087837 | 0.1421215 | 0.0960544 | 0.1288844 |
| $R^2$ | 0.925296 | 0.9627588 | 0.8730759 | 0.9870439 |
| $R^2_{adj}$ | 0.90662 | 0.950345 | 0.8413449 | 0.9838049 |
| $S^2$ | 2.511E−06 | 6.774E−07 | 4.808E−05 | 1.003E−06 |
| *RMSD* | 0.0005282 | 0.0002851 | 0.0023114 | 0.0003338 |

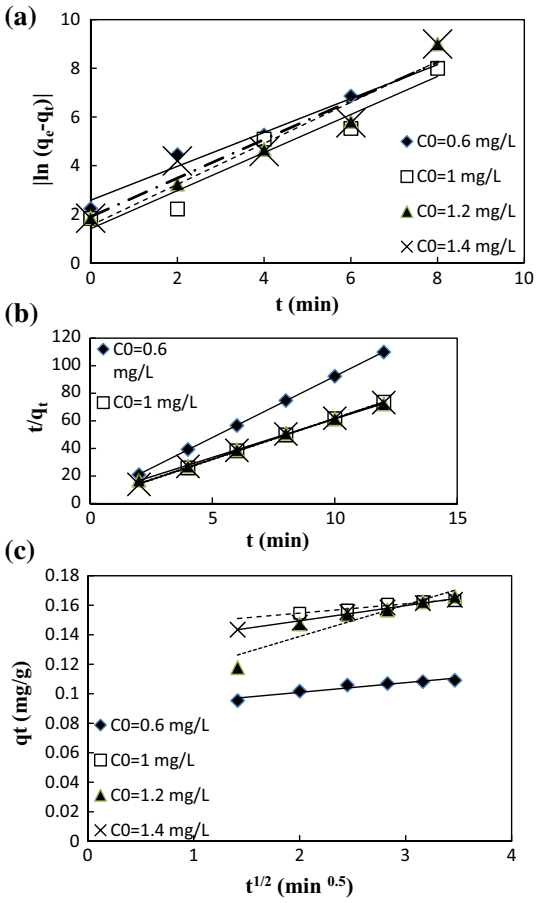


**Fig. 6** **a** Pseudo-first-order kinetic, **b** pseudo-second-order kinetic, and **c** intra-particle diffusion plots for adsorption of PFF onto Fe/Ni bimetallic nanoparticles

### *Pseudo-first-order model*

The pseudo-first-order, or Lagergren first-order, rate equation is widely used for the sorption of a solute from a liquid solution (Jianlong et al. 2001) and is represented as:

$$\ln(q_e - q_t) = \ln(q_e) - k_1 t \quad (13)$$

where $q_e$ is the amount of PFF adsorbed at equilibrium (mg/g); $q_t$ is the amount of PFF adsorbed at time $t$ (mg/g); and $k_1$ is the first-order reaction rate constant (1/min). The pseudo-first-order equation considers the rate of occupation of adsorption sites to be proportional to the number of unoccupied sites.

### *Pseudo-second-order model*

The adsorption kinetics can be described using a pseudo-second-order equation (Wu et al. 2001). The pseudo-second-order kinetic model assumes that the reaction rate is fast at first and becomes slower after reaching equilibrium; the reaction can continue for an extended period at this speed. This model is useful for explaining both non-chemical and non-physical equilibrium and is based on the adsorption capacity of the adsorbent (Febrianto et al. 2009). The differential equation is:

$$\frac{t}{q_t} = \frac{1}{k_2 q_e^2} + \frac{t}{q_e} \quad (14)$$

where $q_e$ and $q_t$ are defined as in the pseudo-first-order model, and $k_2$ is the rate constant of the pseudo-second-order model for adsorption (g/mg min) (Wang and Zhu 2007). Figure 6b plots the linearized form of the pseudo-second-order model at all concentrations studied. The results in Table 2 indicate that the pseudo-second-order kinetic model with larger $R^2$ values is in good agreement with the experimental data than the pseudo-first-order kinetic model. The better fit to the pseudo-second-order model suggests that the adsorption rate is more dependent on the availability of adsorption sites than on the concentration of PFF in solution (Liu et al. 2008).

### *Intra-particle diffusion model*

The intra-particle diffusion model assumes the possibility of adsorbate transport into the pores of the adsorbent via

batch mode adsorption (Sheela and Arthoba Nayaka 2012). The intra-particle diffusion model is expressed as (Demirbas et al. 2002):

$$q = k_i t^{\frac{1}{2}} + C_i \quad (15)$$

where $C_i$ is the intercept that approximates the boundary layer thickness and where a large intercept indicates a greater boundary layer effect, and $k_i$ is the intra-particle diffusion rate constant (mg/g $min^{0.5}$) which can be evaluated from the slope of the linear plot of $q$ versus $t^{\frac{1}{2}}$ (Ozcan et al. 2006).

In this model, the plot of uptake will be linear if intra-particle diffusion is involved in adsorption; if these lines pass through the origin, then intra-particle diffusion is the rate-controlling step. If the plots do not pass through the origin, there is some degree of boundary layer control, and this further shows that intra-particle diffusion is not the only rate-limiting step. Other kinetic models may control the rate of adsorption and could all be operating simultaneously (Hameed and Daud 2008); however, the linear plots at each concentration did not pass through the origin (Fig. 6c; Table 2). This indicates that intra-particle diffusion was not the only rate-controlling step.

## Thermodynamics

The spontaneity of a process can be determined by thermodynamic parameters such as changes in enthalpy ($\Delta H°$), free energy ($\Delta G°$), and entropy ($\Delta S°$). A spontaneous process will show a decrease in $\Delta G$ with an increase in temperature (Ngah and Hanafiah 2008). The thermodynamic parameters of $\Delta G°$ (J/mol), $\Delta H°$ (J/mol), and $\Delta S°$ (J/K mol) are determined using the following relationships:

$$\Delta G^\circ = T\Delta S^\circ - \Delta H^\circ \quad (16)$$

$$\Delta G^\circ = -RT \ln K^\circ \quad (17)$$

$$K^\circ = \frac{q_e}{C_e} \quad (18)$$

$$\ln K^\circ = \frac{-\Delta H^\circ}{RT} + \frac{\Delta S^\circ}{R} \quad (19)$$

where $K°$ is the equilibrium constant, $T$ is the absolute temperature (K), and $R$ is the gas constant. $\Delta H°$ and $\Delta S°$ were obtained from the slope and intercept of plot $\ln K°$ versus $1/T$. Figure 7 shows the effect of temperature on the adsorption of PFF onto Fe/Ni nanoparticles (van't Hoff plot). The observed thermodynamic values are listed in Table 3. The negative value of $\Delta G°$ at all temperatures indicates the spontaneous nature of adsorption of PFF onto Fe/Ni. The negative $\Delta G°$ values indicate that all solutes will remain in the stationary phase rather than in the mobile phase. Solute transfer from the mobile to stationary phase is enthalpically favorable. The positive value of $\Delta S$ indicates

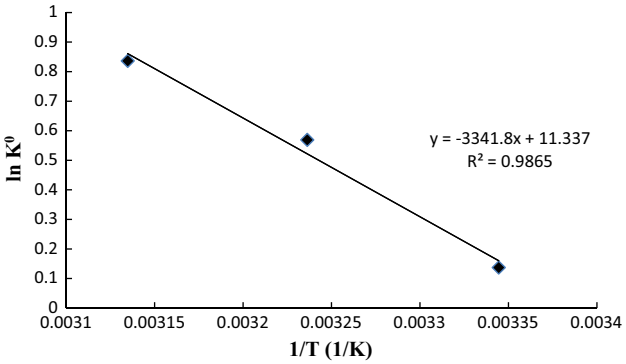


**Fig. 7** Van't Hoff plot for the adsorption of PFF onto Fe/Ni bimetallic nanoparticles

**Table 3** Thermodynamic parameters for the adsorption of PFF on Fe/Ni bimetallic nanoparticles ([PFF] = 0.6 mg/l; Fe/Ni dosage = 1 g/l; pH = 5.73)

| $T$ (K) | $\Delta G°$ (kJ $mol^{-1}$) | $\Delta H$ (kJ $mol^{-1}$) | $\Delta S$ (J $mol^{-1}$ $K^{-1}$) | $R^2$ |
|---|---|---|---|---|
| 298 | −0.341 | 27.79 | 94.25 | 0.9865 |
| 308 | −1.462 | – | – | – |
| 318 | −2.2186 | – | – | – |

the increased randomness at the solid–solution interfaces during adsorption and confirmed the high preference of PFF adsorption onto Fe/Ni. The positive value of the change in enthalpy indicates the endothermic nature of adsorption.

The pseudo-second-order model was identified as the best kinetic model for adsorption of PFF onto the Fe/Ni nanoparticle surface. Accordingly, the rate constant ($k_2$) of the pseudo-second-order model was adopted to calculate the activation energy of adsorption using the following Arrhenius equation (Dogan and Alkan 2003):

$$\ln k_2 = \ln A - \frac{E_a}{RT} \quad (20)$$

where $k_2$ (g/mg min) is the rate constant for the pseudo-second-order adsorption kinetics, $A$ (g/mg min) is the temperature-independent Arrhenius factor, $E_a$ (kJ/mol) is the activation energy, $R$ (8.314 J/mol K) is the gas constant, and the $T$ (K) is the temperature.

The activation energy was determined from the slope of the plot of $\ln k_2$ versus $1/T$ and was 109.57 kJ/mol ($R^2 = 0.9924$) at 298 K for PFF adsorption onto the surface of the Fe/Ni nanoparticles. The magnitude of the activation energy yields information on the physical or chemical nature of adsorption. Physisorption usually has energies in the range of 5–40 kJ/mol; higher activation energies (40–800 kJ/mol) suggest chemisorption (Nollet et al. 2003). The value of the activation energy confirms the nature of the chemisorption of PFF onto Fe/Ni adsorbent.

### Leaching of Ni

Results obtained from the Ni leaching test show when the reaction time increased from 3 to 30 min. No nickel ions could be detected during this short time period. This shows that Fe/Ni bimetallic nanoparticles are stable during the PFF removal.

### MS spectroscopy results of PFF removal

To investigate the PFF removal using Fe/Ni bimetallic nanoparticles, LC/MS analysis was carried out on PFF before and after reaction within 16 min. PFF exhibited a strong peak of $m/z$ at 303 before reaction with the peak area of 1,670,892. Moreover, a very weak peak of $m/z$ at 303 with the peak area of 60,559 confirmed PFF removal using Fe/Ni bimetallic nanoparticles is significant.

## Conclusion

The present study confirms that Fe/Ni bimetallic nanoparticles can be successfully used as an adsorbent for quantitative removal of PFF from aqueous solutions. Equilibrium data were well-fitted to the Langmuir model of adsorption, indicating monolayer coverage of PFF molecules on the outer surface of the Fe/Ni nanoparticles. $R_L$ was 0–1, which confirms that the synthesized Fe/Ni bimetallic nanoparticles were favorable for adsorption of PFF pesticide. The results obtained by comparison of kinetic models of the adsorption system which followed the pseudo-second-order kinetic model suggest that the adsorption rate was more dependent on the availability of adsorption sites than on the concentration of PFF in the solution. Thermodynamic parameters indicate a spontaneous and endothermic process.

**Acknowledgments** The authors gratefully acknowledge the Islamic Azad University, North Tehran Branch, for providing facilities.

## References

Ali I (2010) The quest for active carbon adsorbent substitutes: inexpensive adsorbents for toxic metal ions removal from wastewater. Sep Purif Rev 39:95–171

Ali I (2012) New generation adsorbents for water treatment. Chem Rev 112:5073–5091

Ali I (2014) Water treatment by adsorption columns: evaluation at ground level. Sep Purif Rev 43:175–215

Ali I, Gupta VK (2006) Advances in water treatment by adsorption technology. Nat Lond 1:2661–2667

Ali I, Jain CK (2001) Pollution potential of pesticides in the Hindon river, India. J Environ Hydrol 9:1–7

Ali I, Asim M, Khan TA (2012) Low cost adsorbents for removal of organic pollutants from wastewater. J Environ Manag 113:170–183

Boparai HK, Joseph M, OCarrol DM (2011) Kinetics and thermodynamics of cadmium ion removal. J Hazard Mater 186:458–465

Brijesh SK, Yogesh DS, Abhijit BI, Rajeev CC, Kashinath RP, Chandrashekhar VR (2011) Efficiency and recycling capability of montmorillonite supported Fe–Ni bimetallic nanocomposites towards hexavalent chromium remediation. J Appl Catal B104:407–414

Cordeiro GS, Rocha RS, Valim RB, Migliorini FL, Baldan MR, Lanza MRV, Ferreira NG (2013) Degradation of profennofos in an electrochemical flow reactor using boron-doped diamond anodes. Diam Relat Mater 32:54–60

Demirbas E, Kobya M, Oncel MS, Sencan S (2002) Removal of Ni(II) from aqueous solution by adsorption onto hazelnut shell activated carbon: equilibrium studies. Bioresour Technol 84:291–293

Dogan M, Alkan M (2003) Adsorption kinetics of methyl violet onto perlite. Chemosphere 50:517–528

Edwards CA (1973) Environmental pollution by pesticides. Plenum Press, London, pp 78–79

Fan J, Zhang J, Zhang C, Ren L, Shi Q (2011) Adsorption of 2, 4, 6-trichlorophenol from aqueous solution onto activated carbon derived from loosestrife. Desalination 267:139–146

Febrianto J, Kosasih AN, Sunarso J, Ju YH, Indraswati N, Ismadji S (2009) Equilibrium and kinetic studies in adsorption of heavy metals using biosorbent: a summary of recent studies. J Hazard Mater 162:616-645

Frost RL, Xi Y, He H (2010) Characterization of palygorskite supported zero-valent iron and its application for methylene blue adsorption. J Colloid Interface Sci 341:153–161

Gallo MA, Lawryk NJ (1988) Handbook of pesticide toxicology. In: Hayes Jr WJ, Laws Jr ER (eds) Handbook of pesticide toxicology, Academic Press, New York, pp 917

Gillham RW, O'Hannesin SF (1994) Enhanced degradation of halogenated aliphatics by zero-valent iron. Ground Water 32:958–967

Gonen F, Serin S (2012) Adsorption study on orange peel: removal of Ni(II) ions from aqueous solution. Afr J Biotechnol 11:1250–1258

Gupta VK, Ali I (2001) Removal of DDD and DDE from wastewater using bagasse fly ash, a sugar industry waste. Water Res 35:33–40

Gupta VK, Nayak A (2012) Cadmium removal and recovery from aqueous solutions by novel adsorbents prepared from orange peel and $Fe_2O_3$ nanoparticles. Chem Eng J 180:81–90

Gupta VK, Sharma S, Yadav IS (1998) Utilization of bagasse fly ash generated in the sugar industry for the removal and recovery of phenol and *p*-nitrophenol from wastewater. J Chem Technol Biotechnol 71:180–186

Gupta VK, Ali I, Saini VK (2007) Adsorption studies on the removal of Vertigo Blue 49 and orange DNA13 from aqueous solutions using carbon slurry developed from a waste material. J Colloid Interface Sci 315:87–93

Gupta VK, Gupta B, Rastogi A, Agarwal S, Nayak A (2011) Pesticides removal from waste water by activated carbon prepared from waste rubber tire. Water Res 45:4047–4055

Gupta VK, Kumar R, Nayak A, Saleh T, Barakat MA (2013) Adsorptive removal of dyes from aqueous solution onto carbon nanotubes: a review. Adv Colloid Interface Sci 193–194:24–34

Gupta VK, Nayak A, Agarwal S (2015) Bioadsorbents for remediation of heavy metals: current status and their future prospects. Environ Eng Res 20:1–18

Hall KR, Eagleton LC, Acrivos A, Vermeulen T (1966) Pore-and solid-diffusion kinetics in fixed-bed adsorption under constant-pattern conditions. I & EC Fundam 5:212–223

Hameed BH (2009) Removal of cationic dye from aqueous solutions using jackfruit peel as non-conventional low-cost adsorbent. J Hazard Mater 162:344–350

Hameed BH, Daud FBM (2008) Adsorption studies of basic dye on activated carbon derived from agricultural waste: *Hevea brasiliensis* seed coat. Chem Eng J 139:48–55

Hincapie M, Maldonado MI, Oller I, Gernjak W, Sanchez Perez JA, Ballesteros MM, Malato S (2005) Solar photocatalytic degradation and detoxification of EU priority substances. Catal Today 101:203–210

Hosseini M, Ataie-Ashtiani B, Kholghi M (2011) Nitrate reduction by nano-Fe/Cu particles in packed column. Desalination 276:214–221

Huguet MR, Marshall WD (2009) Reduction of hexavalent chromium mediated by micron- and nano scale zero-valent metallic particles. J Hazard Mater 169:1081–1087

Jabeen H, Iqbal S, Anwar S, Parales RE (2015) Optimization of profenofos degradation by novel bacterial consortium PBAC using response surface methodology. Int Biodeterior Biodegrad 100:89–97

Jianlong W, Xinmin Z, Decai D, Ding Z (2001) Bioadsorption of lead (II) from aqueous solution by fungal biomass of *Aspergillus niger*. J Biotechnol 87:273–277

Liu Y (2008) New insights into pseudo-second-order kinetic equation for adsorption. Colloids Surf A 320:275–278

Liu X, Chen Z, Chen Z, Megharaj M, Naidu R (2013) Remediation of direct black G in wastewater using kaolin-supported bimetallic Fe/Ni nanoparticles. Chem Eng J 223:764–771

Mahboob S, Niazi F, Sultana S, Ahmad Z (2013) Assessment of pesticide residues in water, sediments and muscles of Cyprinus Carpio from Head Balloki in the River Ravi. Life Sci J 10:32–38

Mane VS, Mall ID, Srivastava VC (2007) Use of bagasse fly ash as an adsorbent for removal of brilliant green dye from aqueous solution. Dyes Pigm 73:269–278

Meyer E (2005) Chemistry of hazardous materials. Pearson Prentice Hall, Upper Saddle River

Mourabet M, Rhilassi AE, Boujaady HE, Bennani-Ziatni M, Taitai A (2014) Use of response surface methodology for optimization of fluoride adsorption in an aqueous solution by Brushite. Arab J Chem. doi:10.1016/j.arabjc.2013.12.028

Ngah WW, Hanafiah M (2008) Adsorption of copper on rubber (< i> Hevea brasiliensis</i>) leaf powder: kinetic, equilibrium and thermodynamic studies. J Biochem Eng 39:521–530

Nollet H, Roels M, Lutgen P, Meeren PVD, Verstraete W (2003) Removal of PCBs from wastewater using fly ash. Chemosphere 53:655–665

Ozacar M, Sengil IA (2005) Adsorption of metal complex dyes from aqueous solutions by pine sawdust. Bioresour Technol 96:791–795

Ozcan A, Oncu EM, Ozcan AS (2006) Kinetics, isotherm and thermodynamic studies of adsorption of Acid Blue 193 from aqueous solutions onto natural sepiolite. Colloid Surf A 277:90–97

Perera FP, Rauh V, Tsai WY, Kinney P, Camann D, Barr D, Bernert T, Garfinkel R et al (2003) Effects of transplacental exposure to environmental pollutants on birth outcomes in a multiethnic population. Environ Health Perspect 111:201–205

Phenrat T, Saleh N, Sirk K, Tilto RD, Lowry GV (2007) Aggregation and sedimentation of aqueous nanoscale zerovalent iron dispersions. Environ Sci Technol 41:284–290

Ponder SM, Darab JG, Mallouk TE (2000) Remediation of Cr (VI) and Pb (II) aqueous solution using supported nanoscale zero-valent iron. Environ Sci Technol 34:2564–2569

Ragnarsdottir KV (2000) Environmental fate and toxicology of organophosphate pesticides. J Geol Soc 157:859–876

Rasoulifard MH, Haddadi Esfahlani F, Mehrizadeh H, Sehati N (2010) Removal of C. I. Basic Yellow 2 from aqueous solution by low cost adsorbent: hardened paste of Portland cement. Environ Technol 31:277–284

Saleh TA (2015a) Isotherm, kinetic, and thermodynamic studies on Hg (II) adsorption from aqueous solution by silica-multiwall carbon nanotubes. Environ Sci Pollut Res 22:16721–16731

Saleh T (2015b) Nanocomposite of carbon nanotubes/silica nanoparticles and their use for adsorption of Pb (II): from surface properties to sorption mechanism. Desalin Water Treat. doi:10.1080/19443994.2015.1036784

Saleh TA, Gupta VK (2011) Functionalization of tungsten oxide into MWCNT and its application for sunlight-induced degradation of rhodamine B. J Colloid Interface Sci 362:337–344

Saleh TA, Gupta VK (2012a) Photo-catalyzed degradation of hazardous dye methyl orange by use of a composite catalyst consisting of multi-walled carbon nanotubes and titanium dioxide. J Colloid Interface Sci 371:101–106

Saleh TA, Gupta VK (2012b) Synthesis and characterization of alumina nano-particles polyamide membrane with enhanced flux rejection performance. Sep Purif Technol 89:245–251

Saleh T, Agarwal S, Gupta V (2011) Synthesis of MWCNT/$MnO_2$ and their application for simultaneous oxidation of arsenite and sorption of arsenate. Appl Catal B 106:46–53

Shakerkhatibi M, Mosaferi M, Asghari Jafarabadi M, Lotfi E, Belvasi M (2014) Pesticides residue in drinking groundwater resources of rural areas in the northwest of Iran. Health Promot Perspect 4:195–205

Sheela T, Arthoba Nayaka Y (2012) Kinetics and thermodynamics of cadmium and lead ions adsorption on NiO nanoparticles. Chem Eng J 191:123–131

Shi H, Zhao G, Cao T, Liu M, Guan C, Huang X, Zhu Z, Yang N, Williams O (2012) Selective and visible-light-driven profenofos sensing with calixarene receptors on $TiO_2$ nanotube film electrodes. Electrochem Commun 19:111–114

Singhal RK, Gangadhar B, Basu H, Manisha V, Naidu GRK, Reddy AVR (2012) Remediation of malathion contaminated soil using zero valent iron nano-particles. Am J Anal Chem 3:76–82

Sohrabi MR, Nafiseh Mansouriieh N, Khosravi M, Zolghadr M (2015) Removal of diazo dye Direct Red 23 from aqueous solution using zero-valent iron nanoparticles immobilized on multi-walled carbon nanotubes. Water Sci Technol 71:1367–1374

Sun YP, Li XQ, Zhang WX, Wang HP (2007) A method for the preparation of stable dispersion of zero-valent iron nanoparticles. Colloids Surf A 308:60–66

Sunitha B, Mathew A, Pillai K, Gupta VK (2007) A rapid spectrophotometric assay of some organophosphorus pesticide in vegetable samples. Spectrochim Acta A 67:1430–1432

Taha SM, Amer ME, Elmarsafy A, Elkady MY (2014) Adsorption of 15 different pesticides on untreated and phosphoric acid treated biochar and charcoal from water. J Environ Chem Eng 2:2013–2025

Temkin MJ, Pyzhev V (1940) Recent modifications to Langmuir isotherms. Acta Physiochim URSS 12:217–222

Theron J, Walker JA, Cloete TE (2008) Nanotechnology and water treatment: applications and emerging opportunities. Crit Rev Microbiol 34(1):43–69

Upadhay N, Kumar V, Kumar V (2013) Extraction, UV-visible, FTIR, NMR spectroscopic study of Acephate and effect of pH. Int J Environ Sci 3:1849–1856

Walker GM, Weatherley LR (2001) Adsorption of dyes from aqueous solution - the effect of adsorbent pore size distribution and dye aggregation. Chem Eng J 83:201–206

Wang S, Zhu ZH (2007) Effects of acidic treatment of activated carbons on dye adsorption. Dyes Pigm 75:306–314

Weng X, Lin S, Zhong Y, Chen Z (2013) Chitosan stabilized bimetallic Fe/Ni nanoparticles used to remove mixed contaminants- amoxicillin and Cd (II) from aqueous solutions. Chem Eng J 229:27–34

Wu FC, Tseng RL, Juang RS (2001) Adsorption of dyes and phenols from water on the activated carbons prepared from corncob wastes. Environ Technol 22:205–213

Xu X, Zhou M, He P, Hao Z (2005) Catalytic reduction of chlorinated and recalcitrant compounds in contaminated water. J Hazard Mater 123:89–93

Xu G, Wang J, Mang L (2014) Complete debromination of decabromodiphenyl ether using the integration of Dehalococcoides sp. strain CBDB1 and zero-valent iron. Chemosphere 117:455–461

Zhang Y, Jing Y, Quan X, Liu Y, Onu P (2011) A built- in zero valent iron an aerobic reactor to enhance treatment of azo dye waste water. Water Sci Technol 63:741–746